

Analyst

Accepted Manuscript



This is an *Accepted Manuscript*, which has been through the Royal Society of Chemistry peer review process and has been accepted for publication.

Accepted Manuscripts are published online shortly after acceptance, before technical editing, formatting and proof reading. Using this free service, authors can make their results available to the community, in citable form, before we publish the edited article. We will replace this *Accepted Manuscript* with the edited and formatted *Advance Article* as soon as it is available.

You can find more information about *Accepted Manuscripts* in the [Information for Authors](#).

Please note that technical editing may introduce minor changes to the text and/or graphics, which may alter content. The journal's standard [Terms & Conditions](#) and the [Ethical guidelines](#) still apply. In no event shall the Royal Society of Chemistry be held responsible for any errors or omissions in this *Accepted Manuscript* or any consequences arising from the use of any information it contains.

Cite this: DOI: 10.1039/c0xx00000x

www.rsc.org/xxxxxx

ARTICLE TYPE

Oxidative damage in DNA base revealed by UV Resonant Raman spectroscopy

Francesco D'Amico,^{#a} Francesca Cammisuli,^{b;c} Riccardo Addobbati,^c Clara Rizzardi,^b Alessandro Gessini,^a Claudio Masciovecchio,^a Barbara Rossi,^a and Lorella Pascolo^c

Received (in XXX, XXX) Xth XXXXXXXXX 20XX, Accepted Xth XXXXXXXXX 20XX

DOI: 10.1039/b000000x

We report on the use of UV Raman technique to monitor the oxidative damage of deoxynucleotide triphosphates (dATP, dGTP, dCTP and dTTP) and DNA (plasmid vector) solutions. Nucleotide and DNA aqueous solutions were exposed to hydrogen peroxide (H₂O₂) and iron containing carbon nanotubes (CNTs) to produce Fenton's reaction and induce oxidative damage. UV Raman spectroscopy is shown to be maximally efficient to reveal changes on the nitrogenous bases during the oxidative mechanisms occurring on these molecules. The analysis of Raman spectra, supported by numerical computations, revealed that the Fenton's reaction causes an oxidation of the nitrogenous bases in dATP, dGTP and dCTP solutions leading to the production of 2-hydroxyadenine, 8-hydroxyguanine and 5-hydroxycytosine. No thymine change was revealed in the dTTP solution at the same conditions. Compared to single nucleotides solutions, plasmid DNA oxidation has resulted into a more radical damage that causes the breaking of the adenine and guanine aromatic rings. Our study demonstrates the advantage to use UV Raman spectroscopy for rapidly monitoring the oxidation changes in DNA aqueous solutions that can be assigned to specific nitrogenous bases.

Introduction

The detection of DNA damage for diagnostic screening is an important goal in basic and clinical research. Both normal metabolic processes and environmental factors can cause daily DNA damages, mainly via oxidative stress, resulting in as many as one million molecular lesions per cell per day¹. In addition, the process of DNA replication during cell division is highly prone to errors.

For these reasons the cells have developed a number of mechanisms able to detect and repair the different types of damage that can occur in DNA. Failures in these mechanisms can lead to an accumulation of mutations and damages². For instance, uncorrected lesions in critical genes such as tumor suppressors can increase the possibility of tumoral transformations. In most cases of DNA damage, the nucleobases are chemically modified by the formation of non-native chemical bonds or bulky adducts¹.

The detecting of chemical DNA modifications is the first step towards understanding the genetic damage and repair mechanisms. Many methods and techniques have been developed to qualitatively and quantitatively study DNA damage in bulk materials.

Among the several types of damage source for DNA, the reactive oxygen species (ROS, e.g. superoxide, hydrogen peroxide, and hydroxyl radicals) play an important role³. ROS are produced in cells during normal metabolic processes involving oxygen and they have an important catalytic role. However, when their

production exceeds antioxidant defences, ROS attack and damage cellular components, like proteins, lipids and nucleic acids DNA^{3,4}.

The production of ROS may be significantly increased by exposure to different environmental toxins derived from industry, agriculture, tobacco smoke, or pollution accidents⁵. Cells have many intracellular antioxidant defence mechanisms, but some conditions may cause the failure in the neutralization events. These conditions are considered the initial step for the development of various pathologies. Although DNA is a stable and well-protected molecule, ROS can interact with it and cause several types of chemical changes. Their main effects include the oxidation of DNA nucleobases, de-purination and DNA strand breaks^{5,6}.

Under physiological conditions, the main specie responsible for the genomic damage is the hydroxyl radical (OH•) which induces the generation of a number of DNA base derivatives. Till now, more than 20 different types of oxidative modifications of DNA bases have been identified⁷. The major ROS-induced derivatives of DNA bases are the following: guanine is transformed into 8-hydroxy-guanine, 8-oxo-guanine, and 2,6-diamino-4-hydroxy-5-formamidopyrimidine (FAPy-guanine); adenine is transformed into 2-hydroxyadenine, 8-hydroxyadenine and 4,6-diamino-5-formamidopyrimidine (FAPy-adenine); cytosine is transformed into 5-hydroxycytosine, 5-hydroxyuracil and 5,6-dihydroxyuracil; and thymine is transformed into thymine glycol, 5-hydroxymethyl-uracil and 5-hydroxymethylhydantoin⁵. Furthermore small amounts of OH• also reacts with the sugar portion of nucleic acids leading to the release of intact bases and resulting in chain

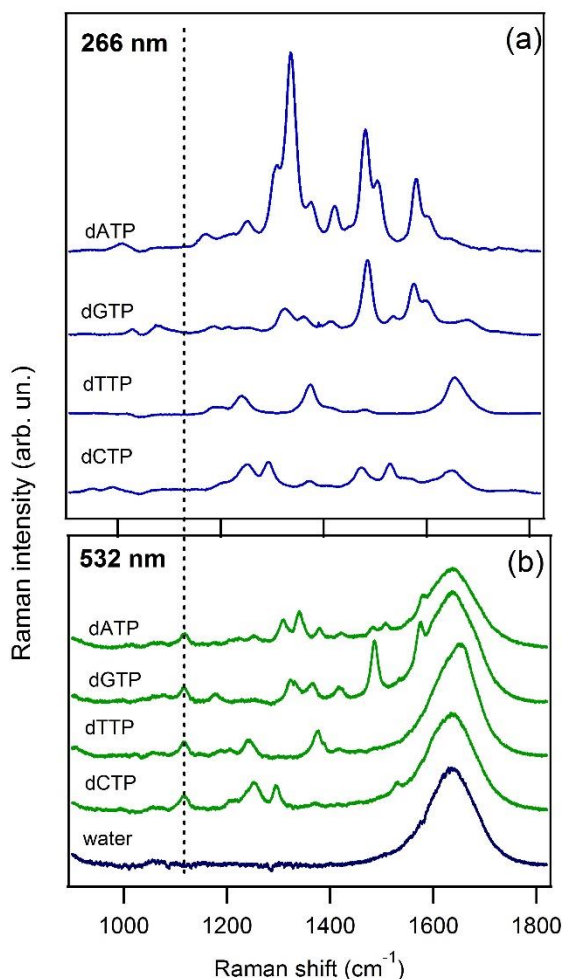


Fig. 1 Panel (a): Resonant Raman spectra of nucleotides aqueous solutions collected at 266 nm of incident wavelength. Spectra are vertically shifted for a better visualization. Panel (b): Raman spectra of the same nucleotides solutions collected at 532 nm. Raman spectrum of pure water has been included for comparison. Spectra are vertically shifted for a better visualization. The dotted line evidences the phosphate stretching band.

breaks^{8,9}.

In nuclear and mitochondrial DNA, 8-hydroxy-deoxy-guanosine is the most frequently studied DNA lesion, because it is an excellent marker for estimating endogenous oxidative DNA damage. In addition, it has been proposed that this molecule is a risk factor for many diseases including cancer. Therefore many protocols for measuring the presence of this molecule in body fluids are currently under development^{8,9}.

Raman spectroscopy has been extensively used in the past years to characterize the chemical structure of DNA^{10,11} and, recently, an advanced set up has been applied to reveal specific changes such as the formation of oxidative products and chain breaks^{12,13}.

The major difficulties in interpreting the Raman spectra of biological macromolecules is the great number of overlapping vibration modes. Furthermore, in the specific case of study of DNA, the analysis of Raman spectra is made difficult by the presence of interfering fluorescence backgrounds which appear by

using incident visible light as exciting radiation. To overcome these difficulties, very interesting DNA damage analysis have been recently performed by exploiting advanced SERS (Surface Enhanced Raman Scattering) and TERS (Tip-Enhanced Raman Scattering) approaches which allow to reveal chain breaks and changes to the phosphate groups of DNA nucleotides^{12,14}.

A limit of SERS and TERS approaches is the impossibility of performing ultraviolet (UV) resonant Raman scattering experiments: UV excitation would allow to perform important structural investigations on DNA because of the $\pi\text{-}\pi^*$ electronic transitions occur at the aromatic rings of the nitrogenous bases¹⁵. Moreover the use of UV excitation instead of the visible one for exciting Raman spectra offers the additional advantage to obtain vibrational spectra without intense fluorescence backgrounds. Furthermore the use of liquid samples, not possible with SERS and TERS, allows to maintain DNA in its natural three-dimensional conformation.

Many articles report on UV Raman spectroscopy experiments performed on nucleotides and DNA products supported by quantum-mechanics simulations which give the theoretical vibrational frequencies of the chemical species under investigation^{11,16-20}. However a complete and consistent analysis carried out with the same computational model for all the several oxidized forms that can be generated from the nucleotides, is presently missing.

In the present work we investigated the chemical changes occurring in nucleotide and DNA bases under stress conditions due to the Fenton's reaction. The study has been performed by exploiting the recently developed UV Raman set-up²¹ at the IUVS beamline of Elettra synchrotron. At the same time, accurate computational simulations were obtained by using an hybrid density functional theory which allowed to recognize the contribution of specific oxidized products in the experimental spectra.

Plasmid DNA (pDNA) was used in our work since it is a simple and practical model able to reproduce the changes that occur in more complex systems, as demonstrated by its many uses in genetic engineering field and biotechnology.

Nucleotides and pDNA oxidations have been produced by Fenton's reaction. This is one of the most important oxidative stress reactions in biological environments since transition metals, copper and especially iron, are abundant in the cells, in part bound to the surface of proteins, or of DNA, and other macromolecules⁸. In our experiments the effects of Fenton's reaction were reproduced by exposing single and mixed nucleotides, and plasmid DNA to pristine carbon nanotubes (containing iron and other metal impurities) and H₂O₂.

We report novel fingerprint Raman features well visible in the spectra excited with UV radiation. These vibrational features specifically identify changes occurring in the DNA bases under oxidant conditions. These results open the possibility to develop novel approaches for determination of DNA damages in biochemical and biomedical studies.

Experimental

Commercial dATP (deoxyadenosine triphosphate), dCTP (deoxycytidine three-phosphate), dGTP (deoxyguanosine three-

Cite this: DOI: 10.1039/c0xx00000x

www.rsc.org/xxxxxx

ARTICLE TYPE

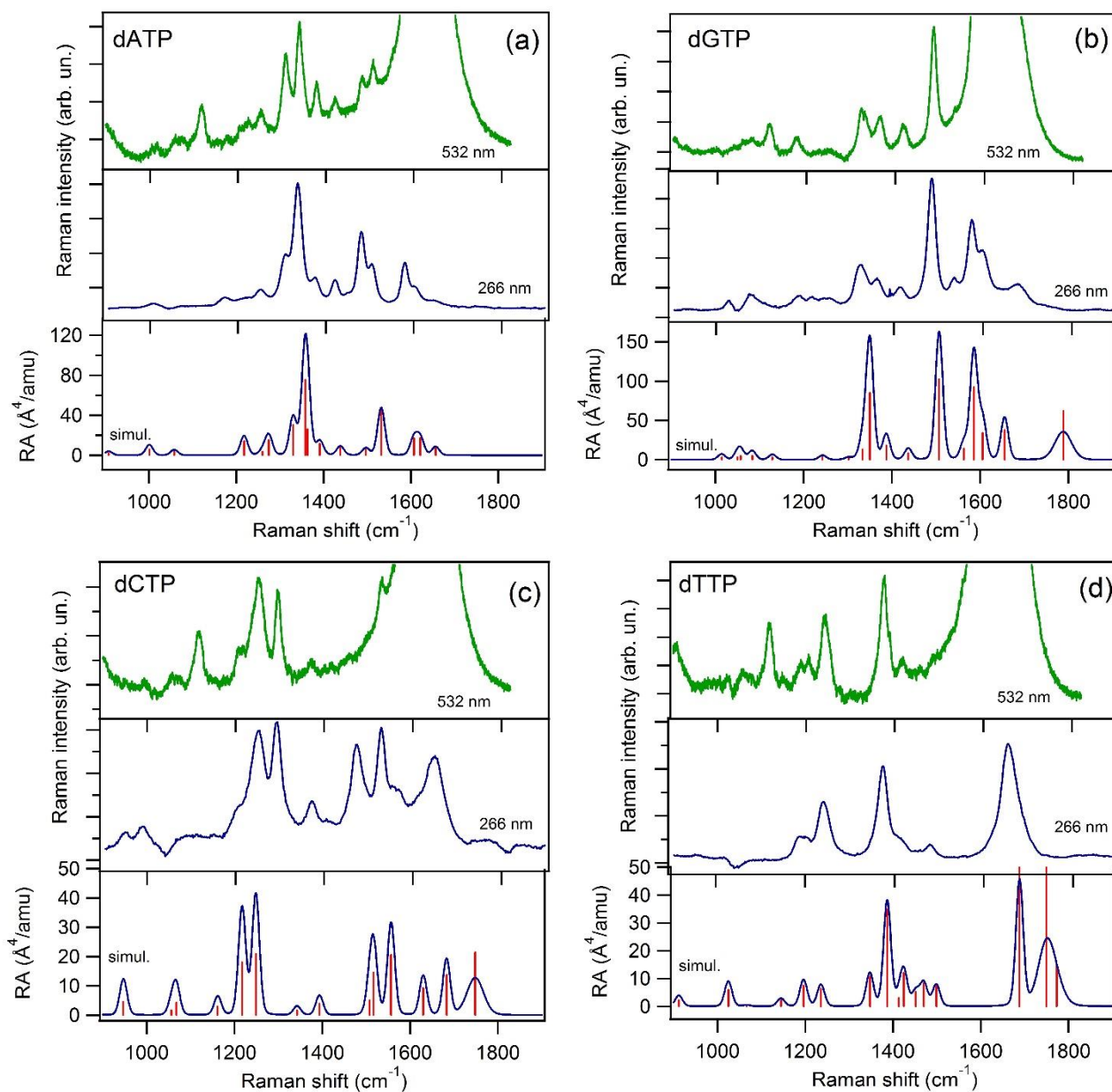


Fig. 2 Raman spectra of dATP (panel a), dGTP (panel b), dCTP (panel c) and dTTP (panel d) collected at 266 and 532 nm of incident radiation, compared with the simulated spectrum of the corresponding nitrogenous bases (simul.). See text for more details

phosphate) and dTTP (deoxythymidine three-phosphate) solution (100mM) were diluted to 10 mM in MilliQwater. Plasmid circular DNA (pUC19 vector)²² was amplified in bacterial cells (DH5 α), then purified with the QIAGEN Plasmid Midi Kit and diluted to a final concentration of 0.5 $\mu\text{g}/\mu\text{l}$. Aliquots of single nucleotide and plasmid DNA samples were incubated on ice for 3 hours with iron containing 5 $\mu\text{g}/\mu\text{l}$ single-walled carbon nanotubes and 1% H₂O₂,

in order to produce oxidation from Fenton's reaction⁸. The incubation/reaction was stopped by removing the carbon nanotubes by centrifugation (7500 x g, 10 minutes) and the samples were immediately measured by Raman. The measurements have been carried out at the IUVS beamline at Elettra synchrotron, in Trieste (Italy). A complete description of the experimental apparatus can be found in D'Amico et al.²¹.

Cite this: DOI: 10.1039/c0xx00000x

www.rsc.org/xxxxxx

ARTICLE TYPE

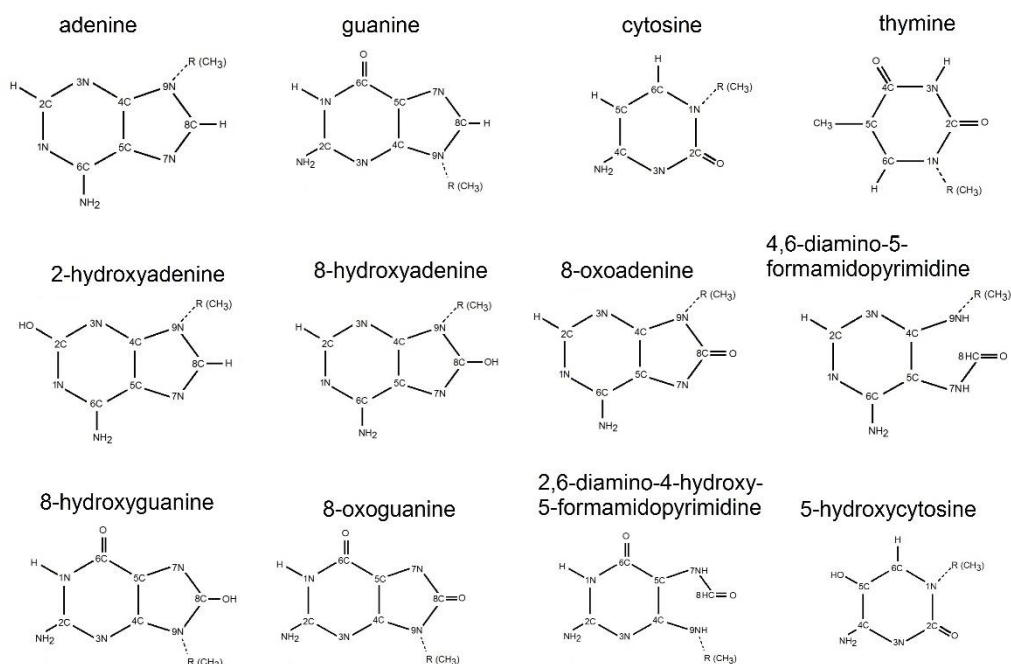


Fig. 3 Schematic representation of the molecular structures used for the simulations.

Excitation sources at 532 nm and 266 nm have been used with the solutions placed in standard quartz cuvettes. Samples were continuously moved during the measurements to avoid decompositions due to the UV exposure. Spectra have been collected in a backscattering configuration employing an $f=750\text{mm}$ Czerny-Turner spectrometer, equipped with an holographic reflection grating of 3600 grooves/mm and a nitrogen-cooled back-thinned CCD.

The incubation/reaction was stopped by removing the carbon nanotubes by centrifugation ($7500 \times g$, 10 minutes) and the samples were immediately measured by Raman. The measurements have been carried out at the IUVS beamline at Elettra synchrotron, in Trieste (Italy). A complete description of the experimental apparatus can be found in D'Amico et al.²¹. Excitation sources at 532 nm and 266 nm have been used with the solutions placed in standard quartz cuvettes. Samples were continuously moved during the measurements to avoid decompositions due to the UV exposure. Spectra have been collected in a backscattering configuration employing an $f=750\text{mm}$ Czerny-Turner spectrometer, equipped with an holographic reflection grating of 3600 grooves/mm and a nitrogen-cooled back-thinned CCD.

The quantum mechanics simulations, carried out to obtain the vibrational frequencies and the Raman scattering activities of the molecules considered in the present work, have been performed by

means of the software package Gaussian-03²³. We used the hybrid DFT model proposed by Becke and co-authors (B3LYP)^{24,25}, where the exchange-correlation function used is the three-parameter Lee-Yang-Parr one²⁶. In addition, we used the basis-set of orbital functions developed by Pople and co-authors that involves the use of spatially diffused p- (hydrogen atoms) and d-polarized (carbon, nitrogen and oxygen atoms) functions^{27,28}.

It has been demonstrated²⁹⁻³³ that the choice of these parameters gives optimal results in predicting the vibrational spectra of aromatic organic molecules against a moderate use of computational resources. The simulated spectra shown in the following sections were obtained from the sum of different Gaussians, one for each vibrational mode derived from the simulations, centred at the frequencies ν_i of the normal modes and with area A_i proportional to

$$A_i = \frac{(\nu_0 - \nu_i)^4 R_i}{\nu_i \left[1 - \exp\left(\frac{h\nu_i}{k_B T}\right) \right]}$$

where R_i is the Raman scattering activity derived from quantum simulations and ν_0 is the frequency of the excitation source³⁴⁻³⁶. The Full width half maximum has been selected to be 20 cm^{-1} and 45 cm^{-1} for the C=O stretching peak, to better fit the experimental lineshape.

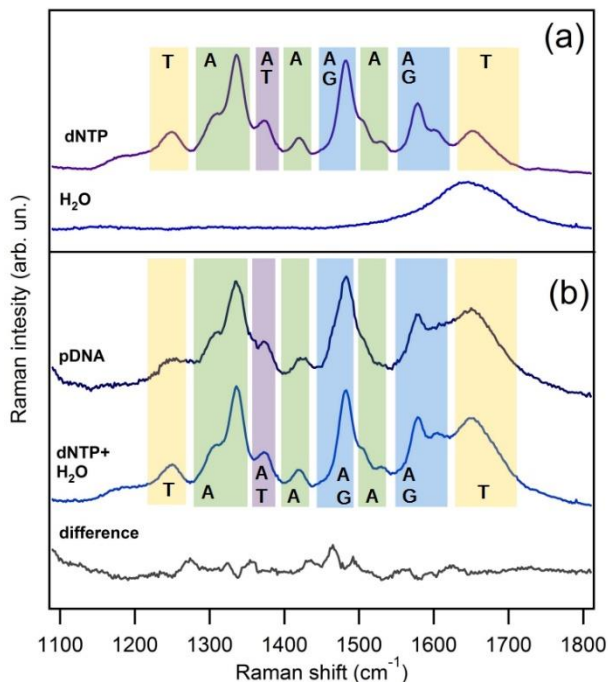


Fig. 4 Panel (a): weighted sum of the Raman spectra of the four nucleotides (dNTP). Colored vertical bars highlights the position of the characteristics band of dATP (A), dGTP (G) and dTTP (T). Panel (b): Raman spectrum of plasmid DNA (pDNA) solution collected at 266 nm of incident radiation. The curve of dNTP+H₂O (see the text for explanations) is still reported, together with the difference spectra between the latter curve and pDNA.

Results and discussion

Fig. 1, panel (a) and (b) respectively, display the Raman spectra of nucleotides in aqueous solutions acquired by using 266 and 532 nm of excitation wavelength. Fig. (b) also shows the spectrum of pure water for a qualitative comparison with the nucleotides spectra. All the spectra recorded at 532 nm exhibit a common feature at 1120 cm⁻¹, which can be assigned to the stretching vibration of the three-phosphate group³⁷⁻³⁹, and the characteristic O-H bending mode of water centred at ≈ 1630 cm⁻¹.

Both these features are almost absent in the Ultraviolet Resonant Raman spectra (UVRR) collected at 266 nm. These are in good agreement and better resolved, with the Raman spectra obtained by others^{15,16} for nucleotides, DNA and RNA. The absence of the phosphate signature in the UVRR spectra (200-300 nm range)^{10,15} allows a better recognition of the vibrational modes associated to nitrogenous bases.

In order to provide a correct assignment of the experimental Raman features, the visible and UV vibrational spectrum of each nucleotide is compared with the theoretical Raman activities obtained for the structure of the four nitrogenous bases (Fig. 2).

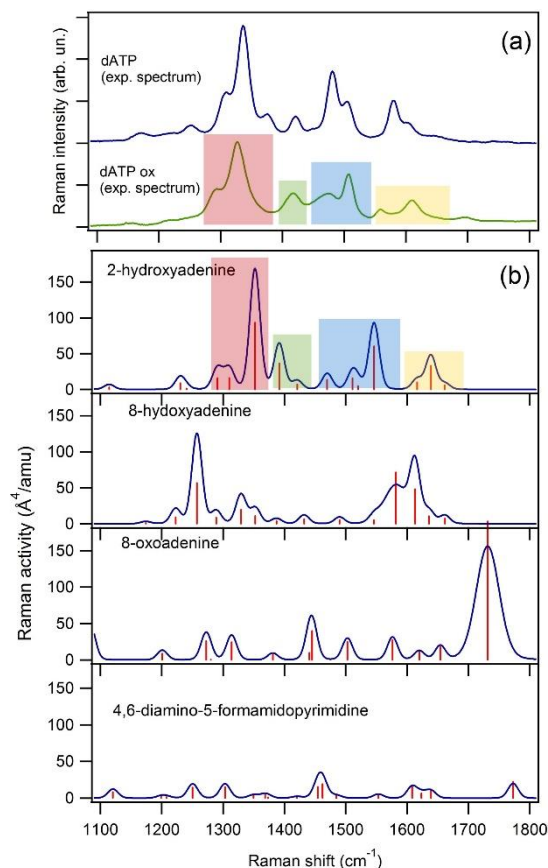


Fig. 5 Panel (a): Raman spectra of dATP solution before (dATP) and after (dATP ox) the Fenton's oxidation process. Panel (b): Simulated spectra of 2-hydroxyadenine, 8-hydroxyadenine, 8-oxoadenine and 4,6-diamino-5-formamidopyrimidine. The colored bars highlight the main vibrational features of the spectra. See text for more details.

35

The frequency and Raman scattering activity (RA) of the vibrational modes of adenine, thymine, cytosine and guanine computed during the simulations are described in Supplementary information (for convenience the atoms positions are indicated in Fig. 3).

The spectra of dATP collected at 532 and 266 nm (panel (a) of Fig. 2) are quite similar, although the observed vibrational peaks exhibit different intensities in the two spectra. The Raman spectrum obtained at 266 nm is dominated by three intense vibrational features centred at 1336, 1481 and 1581 cm⁻¹, respectively. The comparison of experimental profile with the simulated spectrum of adenine (panel a, lower spectrum) allows to assign the first 2 features to the overlapping of C-C and C-N stretching vibrations involving the aromatic rings. The third peak is associated to vibrational stretching modes of the aromatic rings and to many CH₂ scissoring vibrations. It is important to note that the signature at 1581 cm⁻¹ is detectable only in the UV spectrum, due to the absence (or marginal presence) of the O-H water band contribution.

The Raman spectrum of dGTP, collected at 266 nm, is characterized by the appearing of an intense and sharp peak centred at 1485 cm⁻¹ that can be assigned to the C-C and C-N stretching

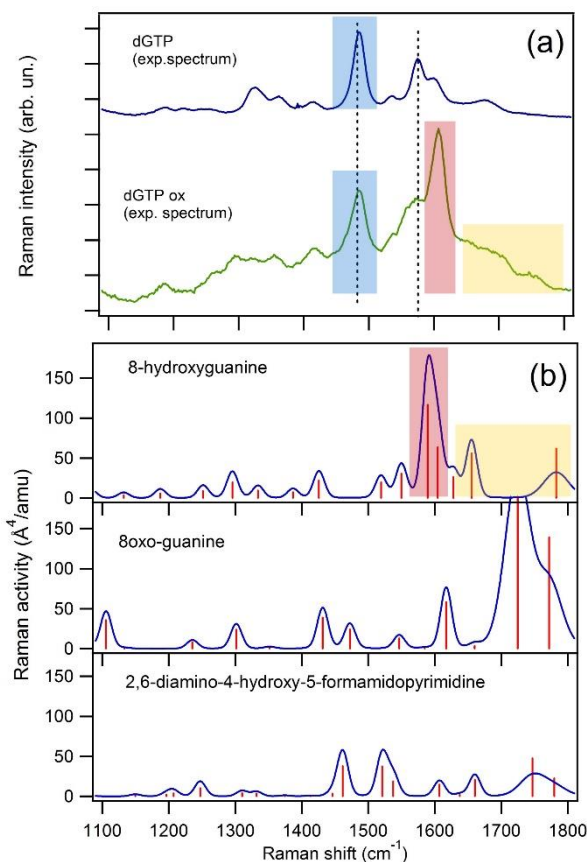


Fig. 6 Panel (a): Raman spectra of dGTP solution before (dGTP) and after (dGTP ox) the Fenton's oxidation process. Panel (b): Simulated spectra of 8-hydroxyguanine, 8-oxoguanine and 2,6-diamino-4-hydroxy-5-formamidopyrimidine. The colored bars highlight the main vibrational features of the spectra. See text for more details

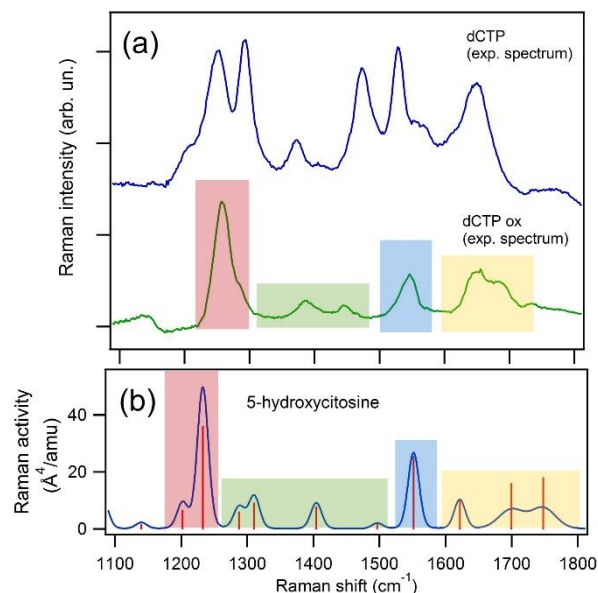


Fig. 7 Panel (a): Raman spectra of dCTP solution before (dCTP) and after (dCTP ox) the Fenton's oxidation process. Panel (b): Simulated spectra of 5-hydroxycytosine. The colored bars highlight the main vibrational features of the spectra. See text for more details

modes involving the aromatic rings, similarly to what observed in dATP spectrum. Another intense feature, centred at 1575 cm^{-1} can be associated to the combination of C-C/C-N bending and CH_2 scissoring vibrations. The 266-excited spectra match with good approximation to the simulated spectra except for the relative intensity which appears higher than expected in the simulated peak at 1343 cm^{-1} . This discrepancy occurs because such vibrations include an asymmetric stretching of the N atom bonded to the deoxyribose. This was not correctly simulated since a simplified model was used in the computational elaboration (CH_3 group instead of sugar group). The feature at 1678 cm^{-1} can be assigned to the C=O stretching mode of dGTP. The broadening of this component is larger with respect to the others and its frequency is significantly lower than the simulated one. Both effects are well known and can be addressed to the HB interactions of carbonyl group with the surrounding water molecules⁴⁰⁻⁴².

The 266 nm-excited spectrum of dCTP (Fig. 1, panel c) exhibits two intense peaks at 1250 and 1292 cm^{-1} which are assigned to the 5C-H and 6C-H bending modes, while the intense peaks found at 1472 and 1528 cm^{-1} are associated to the aromatic ring stretching modes. Finally, the feature centred at 1638 is the result of the overlapping of C=O stretching and NH_2 scissoring vibrations.

30

35

40

45

50

55

60

30

35

40

45

50

55

60

At wavenumber below of 1300 cm^{-1} , the dTTP spectrum shows an unexpected discrepancy between the experiments and the simulations. Both visible and UV Raman spectra exhibit multiple peaks that are clearly underestimated in intensity by the simulations. This may be due to the vibrations of the methyl group added to the base in the simulation that affects the spectra in this wavenumber region. The same effect of methyl group is noted only for thymine and does not affect significantly the computations of the other nucleotides. In the region above 1300 cm^{-1} the simulations match more closely the experimental data. In this spectra range, we identify the peak at 1374 cm^{-1} which is related to the aromatic ring stretching modes, while the intense peak at 1653 cm^{-1} can be assigned to the C=O stretching mode of both the carbonyls present in the structure and to the aromatic ring stretching vibrations.

It is noteworthy that, the spectra of pDNA show also a contribution due to the vibrational modes of water, linked to the low concentration of the solution. Fig. 4(a) shows the Raman spectrum of the plasmid DNA solution, collected using 266 nm excitation source. The panel (b) in the same figure displays the Raman spectrum of pure water, acquired by using the same excitation at 266 nm, together with the curve labelled as dNTP and defined by

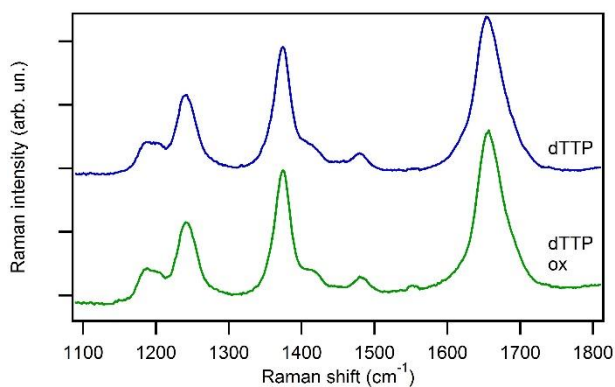


Fig. 8 Raman spectra of dTTP solution before (dTTP) and after (dTTP ox) the Fenton's oxidation process

the following equation:

$$dNTP = \frac{n_{AT}(dATP + dTTP) + n_{CG}(dCTP + dGTP)}{n_{AT} + n_{CG}}$$

where dATP, dTTP, dGTP e dTTP are the Raman spectra reported in Fig. 1(a) and $n_{AT}=1325$ and $n_{GC}=1361$ represent the bases-pairs number contained in the plasmid DNA²². The panel (a) of the same figure shows also the curve dNTP + H₂O, i.e. the profile obtained by the sum of the spectrum of dNTP with the water contribution. The minimal differences observed between the curves pDNA and dNTP + H₂O, (shown in the same panel), demonstrate that the vibrations of the nitrogenous bases are the main contributors in the spectra of the two solutions.

The features coming from different nitrogenous bases in the spectra are highlighted in green (adenine), yellow (thymine) and blue (adenine and thymine) vertical bands. The major contributions, come from adenine and guanine, less significantly from thymine and the features from cytosine are probably hidden by the other (overall) signals.

Fig. 5 points out the spectral changes observed in the dATP solutions under the effects of oxidation. Fig. 5 panel (a) shows the spectra of the aqueous solution of dATP before and after the Fenton's oxidative process, while panel (b) displays the simulated spectra of 2-hydroxyadenine, 8-hydroxyadenine, 8-oxoadenine and 4,6-diamino-5-formamidopyrimidine. The comparison highlights the strong similarities between the experimental spectrum of oxidized dATP and the simulated spectrum of 2-hydroxyadenine. In fact, a similar shape for the structures centred at 1326 cm⁻¹ (highlighted in red in the figure) is found in both the spectra. These vibrational features arise from the C-C/C-N stretching modes within the aromatic rings. The small peak at 1417 cm⁻¹ (shown in green) is addressed to a combination of stretching modes involving the aromatic rings and it is found both in the control (although slightly shifted of 3 cm⁻¹) and oxidized ATP solution. But the real fingerprint match comes from the two structures (evidenced in cyan) between 1472 and 1506 cm⁻¹ that are both caused by the 6-NH₂ scissoring vibrations combined with multiple internal stretching of the aromatic rings. Finally, a good correspondence is found for the peaks at 1560 and 1610 cm⁻¹ (highlighted in yellow) which are due to the 6-NH₂ scissoring

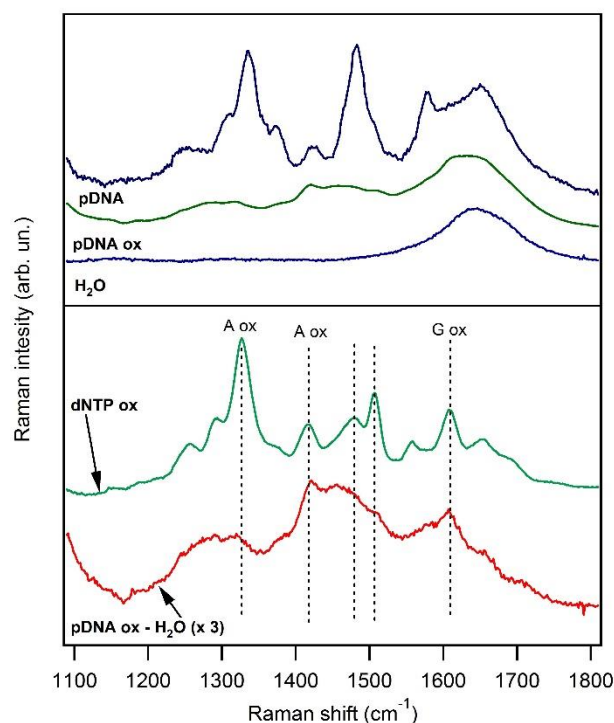


Fig. 9 Panel (a): Raman spectra of pristine (pDNA) and damaged (pDNA ox) plasmid DNA solutions. The spectrum of water is still reported for comparison. Panel (b): Raman spectra of damaged plasmid DNA without the water contribution (pDNA – ox). The curve dNTP ox is still reported for comparison. Vertical dotted lines are guide for the eyes. See text for more details.

modes. The last vibration is shifted lower of 29 cm⁻¹ for the oxidized solution with respect to the same feature from the non-oxidized one (1581 cm⁻¹). It is important to note, however, that although the 2-hydroxyadenine component appears the dominant product, the presence of additional oxidation derivatives is not excluded.

Fig. 6 shows the spectra of the solution of dGTP before and after the oxidative process (panel a), together with the simulated spectra of 8-hydroxyguanine, 8-oxoguanine and 2,6-diamino-4-hydroxy-5-formamidopyrimidine (panel b). The spectra reveal that there is only a limited damage for guanine molecule. This is proven by the persistence of the peak at 1485 cm⁻¹ in the spectrum of the oxidized sample (highlighted in cyan). The most interesting feature of the oxidized spectrum is the presence of an intense peak at 1607 cm⁻¹ (highlighted in red), which can be assigned to the overlapping of two types of vibrations involving respectively C-C/C-H stretching within the aromatic ring and scissoring of the 2-NH₂ atoms. This feature is clearly recognised in the simulated spectra for 8-hydroxyguanine, where this vibrational element is the most intense. The features above 1650 cm⁻¹ and below 1400 cm⁻¹ are hard to assign, due to the overlap of several bands coming from different oxidized species. The smooth band above 1600 cm⁻¹ is probably due to 8-OH group bending modes of the 8-hydroxyguanine 6C=O stretching vibration. Nevertheless, it is not possible to exclude contributions in the spectra arising from 8-oxoguanine and 2,6-diamino-4-hydroxy-5-formamidopyrimidine

C=O stretching vibrations. The superposition of many vibration modes coming from the whole oxidized forms of guanine may also explain the broad shape of the Raman spectrum below 1400 cm⁻¹. In the case of dCTP, the damage found on the sample after the Fenton's reaction process seems to be ascribable entirely to the 5-hydroxycytosine formation. This can be deduced by comparing the simulated spectrum of the latter (Fig. 7 panel (b)) with the experimental spectrum of the damaged dCTP solution (panel a). Specifically, the intense peak at 1257 cm⁻¹ (highlighted in red) can be assigned to the 5-OH group bending on 5-hydroxycytosine. This peak appears to be shifted towards lower wavenumbers of about 35 cm⁻¹ with respect to the same vibrational structure observed in the spectrum of pristine cytosine. The two low intensity features at 1385 and 1444 cm⁻¹ (highlighted in green) can be assigned to a combination of 5-OH bending, 6C-H bending, and C-C/C-N stretching modes occurring within the aromatic ring. Finally, the peak at 1547 cm⁻¹ (highlighted in cyan) can be assigned to 4-NH₂ scissoring vibrations while the large band above 1600 cm⁻¹ can be attributed to the overlapping of vibrational modes involving 4-NH₂ scissoring, 6C-H bending and C-C/C-N stretching modes of the aromatic ring.

Unexpectedly, no changes were detected in the dTTP's Raman spectra before and after oxidation (Fig. 8). This finding suggests that our experimental conditions do not produce chemical changes in this nitrogen base when part of a three-phosphate acid.

Fig. 9 panel (a), reports the spectra of pristine (pDNA) and damaged (pDNA ox) plasmid DNA compared with the water spectrum. Contrary to what happens with nucleotides, the damaged pDNA spectrum intensity is at least three times lower than that of control pDNA (see panel b of Fig. 9). Moreover, it can be noticed that the oxidation observed in the plasmid DNA deviates significantly from the one observed in nucleotide solutions. This is evident in the Fig. 9 panel (b) by comparing the spectrum of the oxidized plasmid DNA (pDNAox) with the curve labelled as dNTP ox, derived from the following equation

$$dNTP_{ox} = \frac{n_{AT}(dATP_{ox} + dTTP_{ox}) + n_{CG}(dCTP_{ox} + dGTP_{ox})}{n_{AT} + n_{CG}}$$

where dATP_{ox}, dGTP_{ox}, dCTP_{ox} and dTTP_{ox} are the oxidized nucleotides spectra shown in the figures 5, 6, 7 and 8 and n_{AT} and n_{CG} are the same coefficients used above for the calculation of the dNTP curve.

The comparison between the pDNA ox spectrum with the curve dNTP ox evidences an almost total disappearance of the peak band centred on 1326 cm⁻¹, characteristic of adenine and found also in the oxidized dATP solution spectra. Similarly, the vibrational bands at 1479 and 1506 cm⁻¹, characteristics of the oxidation of adenine and guanine, are damped in the spectra of oxidized plasmid DNA. These changes suggest that the oxidation of adenine in the DNA is much more drastic than in the dATP solution, causing the break of the aromatic ring at the 8C position with a probable consequent production of derivatives like 4,6-diamino-5-fomamidopyrimidine. A comparable reasoning can be applied to guanosine: although there is a clear fingerprinting for the presence of 8-hydroxyguanosine (1610 cm⁻¹), the intensity of the peak is quite low. This seems to indicate that for this base additional degradations products are formed such as 2,6-diamino-4-hydroxy-5-formamidopyrimidine. The smaller Raman activity observed for

the vibrational modes in 4,6-diamino-5-fomamidopyrimidine and 2,6-diamino-4-hydroxy-5-formamidopyrimidine with respect to the corresponding closed-ring oxidized forms (see Figures 5 and 6) supports our interpretation.

Although the broad shape of the whole spectrum suggests the coexistence of many vibrations added to the ones mentioned above, further peak identification is difficult.

Furthermore it is impossible to detect markers of the oxidation of cytosine, and thymine because of the relative low intensity of the fingerprint band in the total spectrum of both nucleotides mix and DNA.

Conclusions

In the present work we proved the benefit of UV Raman spectroscopy to rapidly obtaining information about the oxidation changes that can be assigned to specific nitrogenous bases in DNA aqueous solutions. Our observations are in accordance and expand the findings of the current literature. The analysis of Raman spectra of nucleotide and plasmid DNA solutions exposed to Fenton's oxidizing reaction demonstrate that the 266 nm excitation wavelength allows to detect efficiently the changes in the nitrogenous bases. Our analysis, when combined with computational simulations reveals that the oxidation on three-phosphate nucleotides in aqueous solutions generates mainly 2-hydroxy-adenine, 8-hydroxy-guanine, (8-oxo-guanine) and 5-hydroxy-cytosine, while 8-hydroxy-guanine is clearly also a product of the DNA oxidation. However, in this case there is a more severe damage of the nitrogenous bases, most probably leading to the opening of the adenine and guanine aromatic rings. This finding is in line with the reported potential production of more than 20 types of DNA oxidation products. The changes occurring in adenine are better traced by UV Raman and this may open to future diagnostic applications, even extending the incident radiation range in the deep UV region.

Notes and references

- ^a Elettra - Sincrotrone Trieste, Strada Statale 14 km 163.5, Area Science Park, I-34149 Trieste, Italy; E-mail: francesco.damico@elettra.eu
^b Institute for Maternal and Child Health, Burlo Garofolo, Trieste, Italy;
^c Department of Medical Science, University of Trieste, Italy
^d Department of Physics, University of Trento, Via Sommarive 14, 38123, Povo, Trento, Italy

† Electronic Supplementary Information (ESI) available: [details of any supplementary information available should be included here]. See DOI: 10.1039/b000000x/

- 1 Y. Jiang and P. E. Marszalek, *Biophys J.*, 2007, **93**, 1758–67.
- 2 S. Clancy, *Nature Education*, 2008, **1**, 103.
- 3 A. Azqueta, S. Shaposhnikov and A. Collins, *Toxicology and Environmental Mutagenesis*, 2009, **674**, 101–108.
- 4 B. Uttara, A. V. Singh, P. Zamboni and R. Mahajan, *Current Neuropharmacology*, 2009, **7**, 65–74.
- 5 K. Roszkowski, *Front. Biosci.*, 2014, **1**, 808–817.
- 6 M. S. Cooke, M. D. Evans, M. Dizdaroglu and J. Lunec, *FASEB J.*, 2003, **17**, 1195–1214.
- 7 S.A. Weitzman, P. Turk, D. H. Milkowski and K. Kozlowski, *Proc. Natl. Acad. Sci. USA*, 1994, **91**, 1261–1264.

- 1 8 T. Hemnani and M. Parihar, *Indian J Physiol Pharmacol.*, 1998, **42**,
2 440–452.
- 3 9 R. Kohen and A. Nyska, *Toxicol Pathol.*, 2002, **30**, 620–650.
- 4 10 J. M. Benevides, S. A. Overman and J. George J. Thomas, *J. Raman*
5 *Spectrosc.*, 2005, **36**, 279–299.
- 6 11 J. George J. Thomas, *Annu. Rev. Biophys. Biomol. Struct.*, 1999, **28**, 1-
7 27.
- 8 12 S. R. Panikkanvalappil, M. A. Mahmoud, M. A. Mackey and M. A. El-
9 Sayed, *ACS Nano*, 2013, **7**, 7524–7533.
- 10 13 V. Sanchez, K. Redmann, J. Wistuba, F. Wubbeling, M. Burger, H.
11 Oldenhof, W. F. Wolkers, S. Kliesch, S. Schlatt and C. Mallidis,
12 *Fertility and Sterility*, 2012, **98**,.
- 13 14 E. Lipiec, R. Sekine, J. Bielecki, W. M. Kwiatek and B. R. Wood,
14 *Angew. Chem. Int. Ed.*, 2014, **53**, 169172.
- 15 15 Z. Q. W. George and J. J. Thomas, *Biopolymers*, 1998, **45**, 247–256.
- 16 16 S. P. A. Fodor and T. G. Spiro, *J. Am. Chem. Soc.*, 1986, **108**,.
- 17 17 L. Chinsky and P. Turpin, *Nucleic Acids Research*, 1978, **5**, 2969-
18 2977.
- 19 18 Z. Dhaouadi, M. Ghomi, J.C. Austin, R.B. Girling, R.E. Hester, P.
20 Mojzes, L. Chinsky, P.Y. Turpin and C. Coulombeau, *J. Phys. Chem.*,
21 1993, **97**, 1074-1084;
- 22 19 A. Toyama, H. Takeuchi and I. Harada, *J. Mol. Struct.*, 1991, **242**, 87.
- 23 20 R. Santamaria, E. Charro- A. Zacarías and M. Castro, *J. Comp. Chem.*,
24 1999, **20**, 511-530,
- 25 25 21 F. D'Amico, M. Saito, F. Bencivenga, M. Marsi, A. Gessini, G.
26 Camisasca, E. Principi, R. Cucini, S. DiFonzo, A. Battistoni, E.
27 Giangrisostomi and C. Masciovecchio, *Nucl. Instr. Meth. Phys. Res.*
28 *A*, 2013, **703**, 33–37.
- 29 22 C. Yaanisch-Perron, J. Vieira and J. Messing, *Gene*, 1985, 103–109
- 30 30 23 Gaussian 03, Revision B.01,
31 M. J. Frisch, G. W. Trucks, H. B. Schlegel, G. E. Scuseria, M. A. Robb,
32 J. R. Cheeseman, J. A. Montgomery, Jr., T. Vreven, K. N. Kudin, J. C.
33 Burant, J. M. Millam, S. S. Iyengar, J. Tomasi, V. Barone, B.
34 Mennucci, M. Cossi, G. Scalmani, N. Rega, G. A. Petersson, H.
35 Nakatsuji, M. Hada, M. Ehara, K. Toyota, R. Fukuda, J. Hasegawa, M.
36 Ishida, T. Nakajima, Y. Honda, O. Kitao, H. Nakai, M. Klene, X. Li,
37 J. E. Knox, H. P. Hratchian, J. B. Cross, C. Adamo, J. Jaramillo, R.
38 Gomperts, R. E. Stratmann, O. Yazyev, A. J. Austin, R. Cammi, C.
39 Pomelli, J. W. Ochterski, P. Y. Ayala, K. Morokuma, G. A. Voth, P.
40 Salvador, J. J. Dannenberg, V. G. Zakrzewski, S. Dapprich, A. D.
41 Daniels, M. C. Strain, O. Farkas, D. K. Malick, A. D. Rabuck, K.
42 Raghavachari, J. B. Foresman, J. V. Ortiz, Q. Cui, A. G. Baboul, S.
43 Clifford, J. Cioslowski, B. B. Stefanov, G. Liu, A. Liashenko, P.
44 Piskorz, I. Komaromi, R. L. Martin, D. J. Fox, T. Keith, M. A. Al-
45 Laham, C. Y. Peng, A. Nanayakkara, M. Challacombe, P. M. W. Gill,
46 B. Johnson, W. Chen, M. W. Wong, C. Gonzalez, and J. A. Pople,
47 Gaussian, Inc., Pittsburgh PA, 2003.
- 48 24 A.D. Becke, *J. Chem. Phys.*, 1993, **98**, 5648.
- 49 25 A.D. Becke, *J. Chem. Phys.*, 1996, **104**, 1040.
- 50 50 26 C. Lee, W. Yang and R.G. Parr, *Phys. Rev. B*, 1988, **37**, 785.
- 51 27 R. Krishnan, J.S. Binkley, R. Seeger and J.A. Pople, *J. Chem. Phys.*,
52 1980, **72**, 650.
- 53 28 M. J. Frisch, A.J. Pople and J.S. Binkley, *J. Chem. Phys.*, 1984, **80**,
54 3265
- 55 55 29 N. Sundaraganesan, S. Ilakiamani, H. Saleem, P.M. Wojciechowski,
56 D. Michalska, *Spectr. Acta A*, 2005, **61**, 2995–3001.
- 57 30 W. Zierkiewicz, D. Michalska and Th. Zeegers-Huyskens, *J. Phys.*
58 *Chem. A*, 2000, **104**, 11685.
- 59 31 D. Michalska, W. Zierkiewicz, D.C. Bienko, W. Wojciechowski, Th.
60 Zeegers-Huyskens, *J. Phys. Chem. A*, 2001, **105**, 8734.
- 32 W. Zierkiewicz, D. Michalska, B. Czarnik-Matusewicz and M.
Rospenk, *J. Phys. Chem. A*, 2003, **107**, 4547.
- 33 P. M. Wojciechowski, W. Zierkiewicz, D. Michalska and P. Hobza, *J.*
Chem. Phys., 2003, **118**, 10900.
- 65 34 K. Chaitanya, C. Santhamma, K. V. Prasad and V. Veeraiah, *J. At.*
Mol. Sci., 2012, **3**, 1-22.
- 35 P. L. Polavarapu, *J. Phys. Chem.*, 1990, **94**, 8106.
- 36 G. Keresztury, S. Holly, J. Varga, G. Besenyi, A.Y. Wang, and J. R.
Durig, *Spectrochim. Acta A*, 1993, **49**, 2007.
- 70 37 R. Jenkins, R. Tuma, J. Juuti, D. Bamford and G. T, *Biospectroscopy*,
1995, **5**, 3–8.
- 38 P. Carey, *Biochemical Applications of Raman and Resonance Raman*
Spectroscopy, Elsevier, 1982.
- 39 Y. Guan, C. J. Wurrey and G. J. T. Jr, *Biophys J.*, 1994, **66**, 225–235.
- 40 F. D'Amico, F. Bencivenga, A. Gessini, E. Principi, R. Cucini and C.
Masciovecchio, *J. Phys. Chem. B*, 2012, **116**, .
- 41 T. Nakabayashi, K. Kosugi and N. Nishi, *J. Phys. Chem. A*, 1999, **103**,
8593–8603.
- 42 N. Nishi, T. Nakabayashi and K. Kosugi, *J. Phys. Chem. A*, 1999, **103**,
80 10851–10858.